Check for updates

From binary AB to ternary ABC supraparticles†

E. Deniz Eren, ‡[a] Mohammad-Amin Moradi,[a] Mark M. J. van Rijt,[a]
Bernette M. Oosterlaken, [a] Heiner Friedrich [ab] and Gijsbertus de With *[a]

Control over the assembly and morphology of nanoscale functional building blocks is of great importance to hybrid and porous nano-materials. In this paper, by combining different types of spherical nanoparticles with different size ratios in a hierarchical assembly process which allows us to control the final structure of multi-component assemblies, we discuss self-assembly of an extensive range of supraparticles, labelled as AB particles, and an extension to novel ternary particles, labelled as ABC particles. For supraparticles, the organization of small nanoparticles is known to be inherently related to the size ratio of building blocks. Therefore, we studied the formation of supraparticles prepared by colloidal self-assembly using small silica nanoparticles (SiO_2 NPs) attached on the surface of large polystyrene latex nanoparticles (PSL NPs) with a wide size ratio range for complete and partial coverage, by controlling the electrostatic interactions between the organic and inorganic nanoparticles and their concentrations. In this way hierarchically ordered, stable supraparticles, either fully covered or partially covered, were realized. The partially covered, stable AB supra-particles offer the option to create ABC supraparticles of which the fully covered shell contains two different types of nanoparticles. This has been experimentally confirmed using iron oxide (Fe_3O_4) nanoparticles together with silica nanoparticles as shell particles on polystyrene core particles. Cryo-electron tomography was used to visualize the AB binary and ABC ternary supraparticles and to determine the three-dimensional structural characteristics of supraparticles formed under different conditions.

New concepts

Supraparticles composed of organic core and layer of inorganic nano-particles are of considerable interest in academia and industry. Under the proper process conditions, individual nanoparticles can cluster together to form defined hybrid structures. However, understanding the precise formation of supraparticles having different sizes and types of nano-particles and simultaneously tuning the coverage of inorganic particles is still a challenge due to the necessity of adjusting the interplay between attractive and repulsive dynamic forces of nanoparticle systems. Key is therefore to achieve full control over the interactions between nano building blocks to precisely and simultaneously direct the nanostructure of supraparticles. To address these challenges, we utilized smaller spherical silica and iron and larger polystyrene latex nanoparticles with different sizes. With the help of advanced tools such as cryo-electron microscopy and cryo-electron tomography, the nanostructure of smaller particles as a function of the size ratio between nano building blocks was studied and analysed. Furthermore, cryo-TEM was used to monitor and capture the formation of stable partially covered binary supraparticles at different concentrations and help us to understand the formation mechanism of binary and ternary supraparticles. Our paper provides a design strategy to form ternary supraparticles. As the formation of supraparticles with either binary or ternary characteristics is fundamentally controlled by the principles of physical chemistry, the route presented in our paper can be utilized to initiate the formation of supraparticles for a wide range of nano building blocks with different sizes, compositions, and shapes which eventually could be an enabler for the next generation hybrid materials with a myriad of applications.

[a] *Laboratory of Physical Chemistry and Center for Multiscale Electron Microscopy, Department of Chemical Engineering and Chemistry, Eindhoven University of Technology, Eindhoven, The Netherlands. E-mail: G.deWith@tue.nl*

[b] *Institute for Complex Molecular Systems, Eindhoven University of Technology, Eindhoven, The Netherlands*

† Electronic supplementary information (ESI) available. See DOI: **https://doi.org/ 10.1039/d2mh00574c**

‡ Present address: Department of Chemistry, McGill University, 801 Sherbrooke Street West, Montreal, Quebec H3A 0B8, Canada.

In the past decade tremendous progress was made in making functional inorganic nanoparticles having a wide range of properties including size, shape, composition, and surface chemistry. These properties of inorganic nanoparticles are used in various areas of science and technology, such as sensing,[1,2] catalysis,[3] electronics,[4,5] biomedicine,[6] magnetics[7] and optics.[8,9] Therefore, precisely tunable morphology, composition, size, and shape of the inorganic nanoparticles will enable the exploitation of their tremendous potential.

The assembly of complex supraparticles, defined as building blocks that comprise a core (nano)particle covered by smaller

nanoparticles, from individual organic and inorganic building blocks allow scientists to explore uncharted areas of, hopefully enhanced, material properties and is of large interest for engineering applications.[10–13] Over the last decades, a tremendous effort has been devoted to design and produce these hybrid nanoparticles that combine well-defined geometries with a substantial complexity and resulted in interesting morphologies and tunable properties.[14–17] Furthermore, if this complexity covers both compositional and interfacial anisotropy, such tailor-made hybrid nanoparticles can pave the way for structures that cannot be obtained by simply mixing their individual elements.[18,19] The self-assembly of colloidal particles can be controlled by altering the geometry, shape, or topology of the particles, by modifying the attractive forces between two different types of particles, or by confining them onto a curved surface.[17]

Two basic routes to attach nanoparticles to polymeric particles have been developed, namely *ex situ* and *in situ* approaches. The *in situ* approaches rely on the synthesis of nanoparticles from inorganic precursors that assemble on preformed polymeric particles. A myriad of hybrid nanoparticles were synthesized this way using various polymeric particles.[20,21] However, a major drawback of this approach is that it results in wide size distributions. On the other hand, the *ex situ* approaches make use of the controlled assembly of inorganic and polymeric nanoparticles that are both preformed and it has been shown in the literature that raspberry-like supraparticles can be obtained from binary mixtures of oppositely charged colloids by using two different components.[22–25] Almost 40 years ago Vincent *et al.* laid the ground for this field of adsorption of oppositely charged small particles onto larger particles by utilizing colloidal self-assembly of individual nanoparticles at different electrolyte concentrations *via* electrostatic interactions.[26,27] Ever since then electrostatic interactions between small and larger nanoparticles have been exploited to create binary supraparticles from inorganic and organic nanoparticles. In one of the early examples, Dokoutchaev *et al.* demonstrated the assembly of different nano-scale metallic particles onto larger polystyrene particles, thereby providing an excellent example of the flexibility of the colloidal self-assembly approach to create supraparticles with different components.[28] Many other groups employed the same strategy throughout the years by using different types of inorganic nanoparticles such as gold,[29,30] silica[31,32] hematite[33] and silver.[34] However, it is crucial to mention that while Zanini *et al.* demonstrated the formation of micrometer size supraparticles having two different sizes of silica nanoparticles coexisting on the surface of another larger silica particle,[35,36] to the best of our knowledge, no other group was able to demonstrate the coexistence of different inorganic nanoparticles on the surface of a single core particle so far.

Assembly of small particles on a curved larger particle is a complex and interesting phenomenon.[37–39] If the assembly of (similar size) spherical particles is initiated on a flat surface, they will pack preferably into a hexagonal arrangement, meaning that these particles have in principle six nearest neighbors. If one maps this arrangement on a sphere, it is well-known that such a map is impossible, unless some non-six coordinations are introduced.[17,37] C$_{60}$ fullerenes[40,41] and soccer balls[42] are

typical examples of this phenomenon,[43] showing 12 pentagonal and 20 hexagonal patches. Moreover, as the number of particles on the sphere increases, additional dislocations are introduced, which consist of pairs of 5–7 line dislocations.[39] Bausch *et al.* investigated very large systems by initiating the assembly of similar sized microspheres onto an emulsion droplet.[38,39] They demonstrated that with increasing size ratio indeed mainly six coordinated centers are present with a certain number of compensating dislocations (5–7 defects, or as they called them, grain boundary scars).

Cryo-transmission electron microscopy (cryoTEM) and cryo-electron tomography (cryoET) provide powerful and robust means to visualize and characterize organic, inorganic and hybrid nanoparticles.[44] These cryo-electron microscopy techniques involve image acquisition of the sample of interest in a frozen state which allows the visualization of different (nano)particles as they exist in solution.[45–48] Two-dimensional (2D) CryoTEM offers a direct and relatively easy way to visualize the structural characteristics of nanomaterials. While the structural characteristics of hybrid nanomaterials can be assessed with 2D CryoTEM images, a detailed and quantifiable determination of a three-dimensional (3D) structure requires cryo-ET,[49–54] which involves collecting a tilt-series of 2D projection images for a feature of interest, which can be utilized to generate a 3D tomogram. CryoET involves tilting the specimen through an angular range of typically −70° to +70° and collecting a tilt series of 2D projection images from a feature (in this context a hybrid nanoparticle) of interest. For every single CryoTEM sample the electron dose is a crucial factor that must be adjusted and controlled to avoid damaging the sample and failing to do so will most likely results in losing structural details. As the structural complexity of hybrid nanoparticles increases, it will become even more critical to unravel the structural details. For all these reasons, it is not hard to predict that cryo-TEM derived 2D and 3D information will play a significant role in understanding the fine structural details of next generation hybrid nanoparticles with improved and specialized functionality.

We recently showed that a certain type of supraparticles based on polystyrene and silica, called nano-raspberries, can lead to materials with a complex hierarchy.[55] Moreover, we also demonstrated the inherent reversibility of supraparticles (dis)-assembly by dynamically controlling the interaction forces between the two components.[25]

Here we study spherical silica and iron oxide nanoparticles and the effect of concentrations and pH on the degree of and the maximum coverage of larger core particles. Moreover, we show that not only binary supraparticles (referred to as AB particles) but also ternary supraparticles (referred to as ABC particles) can be realized. First, for a wide range of binary assemblies, we discuss the formation of supraparticles by utilizing different sizes of fundamental building blocks and effect of size ratio on the organization of small nanoparticles on the surface of large nanoparticles. Thereafter, we take our design strategy one step further and create ternary ABC supraparticles for which we discuss the governing principles of the self-assembly by benefiting from DLVO and Flory–Huggins theories. For the ABC supraparticles, core PSL particles are first

partially but stably covered with one type of either silica or magnetite nanoparticles and subsequently with another type of colloidal particles. Depending on the type of inorganic nanoparticle that was used to create partially covered supraparticles, we used either a different size of silica or magnetite. As the formation of supraparticles with either binary or ternary characteristics is fundamentally controlled by the principles of physical chemistry, our strategy can be exploited to create supraparticles for a wide range of inorganic and organic nanoparticles with different sizes, compositions and shapes which eventually could be an enabler for the next generation composite materials with a myriad of applications. Options for applications are, for example, their use as raw materials for obtaining materials with well-controlled microstructure, for instance, controlled porosity by removal of the polymer particles, and realizing conducting materials by controlling their percolation behavior.

As inorganic building blocks silica nanoparticles and (commercially available) iron oxide nanoparticles were used to create either binary (AB) or ternary (ABC) supraparticles on (commercially available) polystyrene core particles. Here we discuss the characteristics of the building block particles, while in the sections hereafter we deal with the AB and ABC supraparticle formation.

As indicated in the experimental section, silica nanoparticles with controlled size were synthesized according to the previously reported work by Yokoi et al.[56] and Carcouët et al.[47] There are many advantages of this method, but the most important one is the excellent control over the size of silica nanoparticles. CryoTEM results indeed confirmed that the diameter of the as-synthesized silica nanoparticles is well-controlled (Fig. S1a and b, ESI†) and in line with the results obtained from DLS size measurements (Fig. S1c, ESI†). As-synthesized SiO_2 NPs are inherently negatively charged[47] (Fig. S1d, ESI†) and therefore one must, in order to initiate the formation of supraparticles, modify the surface of the as-synthesized SiO_2 NPs, which was achieved by reaction with functional silanes according to a procedure reported by Pham et al.[57] After surface modification, cryoTEM was conducted to determine any possible alterations in the size of the SiO_2 NPs. The cryoTEM results indicate that the size of SiO_2 NPs was not altered upon surface modification (Fig. S1c, ESI†); however, DLS measurements show a slight increase in hydrodynamic diameter from 24 to 27 nm, probably due to the presence of the functional groups on the surface of SiO_2 NPs[58] as the contour length of APTES is 1.5 nm[59,60] (Fig. S5, ESI†). Such coverage with organic molecules having a low density is nearly impossible to detect with cryoTEM. As the formation of supraparticles depends on the attractive interactions between two components, zeta potential measurements were conducted to investigate the alterations in the surface charge of the SiO_2 NPs following surface modification. For as-synthesized SiO_2 NPs, a negatively charged nature is demonstrated at pH 2, while zeta potential measurements after surface modification indicate positively charged particles (Fig. S1d, ESI†).

The iron oxide nanoparticles (Fe_3O_4 NPs) and other silica nanoparticles which used to create ternary ABC supraparticles measured to have a diameter of 29 ± 0.7 nm and 11 ± 1.1 nm, respectively (Fig. S4, ESI†). The sizes of the iron oxide and silica

nanoparticles are reported as mean $\pm$ standard deviation of the mean. Commercial polystyrene latex nanoparticles with diameters of 80 nm, 100 nm, 140 nm, 170 nm and 450 nm were characterized by employing the same methods described above to determine the size and surface charge. While the cryoTEM results (Fig. S1e, ESI†) indicated that the diameter of the PSL NPs was in line with those obtained from DLS size measurements (Fig. S1c, ESI†), zeta potential measurements showed that PSL nanoparticles are negatively charged (Fig. S1d, ESI†). To initiate the formation of supraparticles, the dispersions containing either SiO_2 NPs or Fe_3O_4 NPs were gently mixed with the PSL NPs and the pH was lowered to 2, where either the SiO_2 NPs or the Fe_3O_4 NPs can form supraparticles with the PSL NPs due to the attractive electrostatic forces.[25] CryoTEM results of the binary supraparticles created after adsorption of SiO_2 NPs on the surface of PSL NPs are shown in Fig. 1a–e.

In this section we focus on binary supraparticles with a high surface coverage of SiO_2 NPs having wide size range, as can be seen in various cryoTEM images (Fig. 1a–e). To confirm that binary AB supraparticles are indeed three-dimensional assemblies, cryo-electron tomography (cryoET) was conducted. From the cross-sectional cryoET reconstructions at different tilt angles, it is clear that SiO_2 NPs are attached over the whole surface of the PSL nanoparticles (Fig. 1f–j).

To assess how many SiO_2 NPs can be attached on the surface of PSL NPs, a theoretical estimate given by Mansfield et al.[61] was employed. These authors studied, taking the radius of the large sphere r_1 much larger than that of the small sphere r_2, i.e. $r_1 > r_2$, how many "probe" (small) spheres on average would become attached to a "target" (large) sphere if the process continues until all available sites are exhausted on the surface of the target sphere. This was done by either allowing mobility of the small sphere over the large sphere or not, only leading to small differences in terms of maximum coverage. As will be elaborated on why later, we use here the result for immobile small spheres after attachment. According to Mansfield et al.
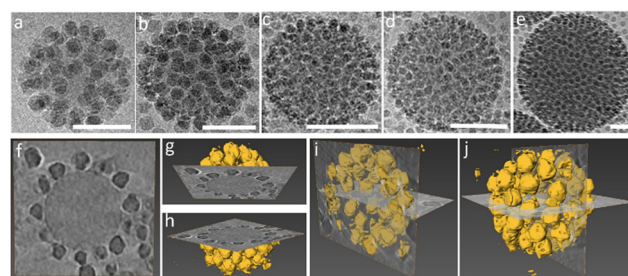

Fig. 1 CryoTEM analysis of different types of supraparticles made by adjusting the size ratio of surface-modified silica nanoparticles and polystyrene latex nanoparticles at pH 2. (a) L_{80}/S_{24}, $r_1/r_2 = 3.3$, (b) L_{120}/S_{21}, $r_1/r_2 = 5.7$, (c) L_{140}/S_{10}, $r_1/r_2 = 14$, (d) L_{170}/S_{10}, $r_1/r_2 = 17$, and (e) L_{400}/S_{30}, $r_1/r_2 = 13.3$. Here L_{xx} and S_{xx} indicates the size xx nm of the PSL NPs and Silica NPs used and r_1/r_2 their size ratio. Scale bars: 100 nm. (f–j) Further 3D reconstruction of a supraparticle demonstrating that a single PSL NP is fully covered by silica NPs.
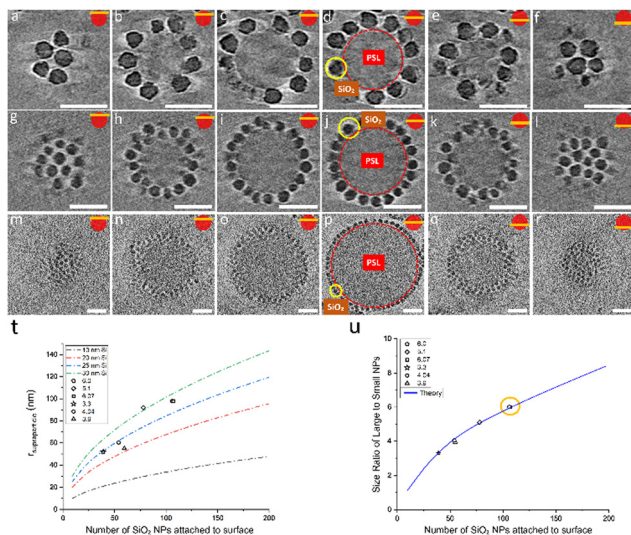
Fig. 2 Cross-sections at different heights in supraparticles as obtained from cryoET reconstructions and having size ratios $r_1/r_2 = 3.3$ (a–f), $r_1/r_2 = 5.6$ (g–l) and $r_1/r_2 = 18.4$ (m–r) show that the PSL nanoparticles are fully covered with SiO_2 NPs. Scale bars: 100 nm. Further (t) shows the supraparticle radius *versus* number of attached particles, (u) demonstrates the size ratio of large to small nanoparticles *versus* number of attached particles to the surface. The encircled data point is discussed in the main text as an example.

the mean number of the small spheres M that can be attached is given by

$$M = K \left(\frac{r_1}{r_2} + 1 \right)^2$$

with the constant $K = 2.187 \pm 0.004$.[61] We calculated M for supraparticles made by using different size ratios and compared the result with the experimental results obtained from cryoET (Fig. 2, SM1–3). The above-mentioned formula is highly sensitive to the size ratio of the individual building blocks which is reflected in the experimental system, where, although the nanoparticles are highly monodisperse, some average size variation exists between batches. While in Fig. 2a–f the radius of SiO_2 NPs used to form supraparticles is 12 ± 0.6 nm, in Fig. 2g–r the radius is 14 ± 0.45 nm (ESI†). Although the difference seems small, the effect is significant upon calculating the coverage of SiO_2 NPs attached to the surface of PSL NPs. As the radius of separate PSL NPs in different systems used in our study ranged between 40 nm and 225 nm, the coverage (number of covering nanoparticles on the surface of the core particle) varied between 40 and 585. Upon comparing the experimental results with the theoretical estimates, it appears that the number of SiO_2 NPs attached to the surface of PSL NPs as a function of size ratio can be predicted quite accurately (Fig. 2t and u). While different plots in Fig. 2t (green for 30 nm, blue for 25 nm, red for 20 nm and black for 10 nm) indicate the estimated number of small nanoparticles on the surface of a large nanoparticle based on theoretical estimate given by Mansfield *et al.*, data points (star for size ratio of 3.3, triangle for 3.9, circle for 4.04, rhombus for 5.1, pentagon for 6.0, and square for 6.07)

show 6 different supraparticles analysed in this study. As an example, for the size ratio of large to small nanoparticle $r_1/r_2 = 6.07$, the theory predicts that $M^{\text{theor}} = 109.3$, while cryoET results demonstrate that $M^{\text{exp}} = 107$ (Fig. 2u – orange circle). The agreement between the experimental and theoretical M-values is also a good indicator that equilibrium was reached.

After confirming that the number of SiO_2 NPs attached to the surface of the PSL NPs corresponds to maximum packing density achievable on a spherical surface for specific size ratio, we proceeded by analyzing the arrangements of SiO_2 NPs on the surface of PSL nanoparticles. To that purpose, cryoET was conducted for several AB supraparticles with different size ratios, followed by extraction of the positional information and coordination number (CN), *i.e.* the number of nearest-neighbors, for all SiO_2 NPs. The positions of small SiO_2 NPs were determined by acquiring projection images at different angles and by combining these different images in order to construct a set of 3-D coordinates for all SiO_2 NPs covering a PSL NP.

Our analysis indicates that for different size ratios of small and large nanoparticles, the SiO_2 NPs were arranged in different configurations (Fig. 3). For the smaller size ratios CNs of 3, 4, 5, 6, 7 and 8 occurred as on a sphere there must be additional defects,[37,62] whereas for the largest size ratio only CN = 5 and CN = 7 grain boundary-like line dislocations were found. This is in line with what was demonstrated by Bausch *et al.*[39] who experimentally showed that owing to the curvature of the large
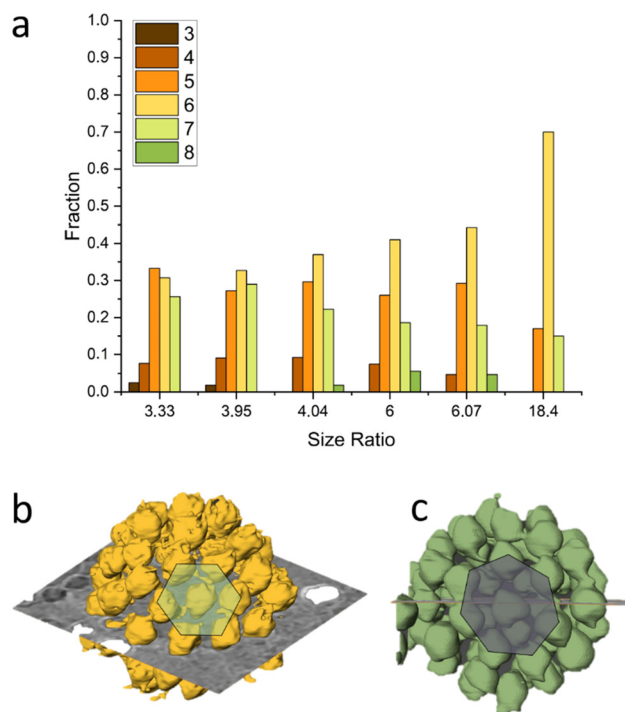

Fig. 3 Organization of silica nanoparticles on the surface of polystyrene latex nanoparticles showing the CNs as a function of size ratio r_1/r_2 (a). For size ratios (r_1/r_2) 3.33, 3.95, 4.04, 6, 6.07, and 18.4 the number of SiO_2 NPs attached to the PSL NPs are 39, 54, 55, 106, 107, and 585, respectively. An example of a hexagonally coordinated SiO_2 NP is shown in (b) and an example of a seven-fold coordinated SiO_2 NP in (c).

core particle, the coordination of small particles on the surface of the large one must incorporate the topological defects. They illustrated this phenomenon using particles with a size between 6–24 μm and showing that as the particle size ratio increases, point defects (CN = 3 or 4) become energetically costly and instead linear dislocations are formed. From our results as shown in Fig. 3, it is clear that upon increasing the size ratio between SiO_2 NPs and PSL NPs, the fraction of CN = 6 configurations for these systems with a few orders of magnitude smaller size, also increases.

In above sections by creating AB supraparticles, the maximum number of small nanoparticles (SiO_2 NPs) on the surface of a large particle (PSL NPs) were calculated and translated experimentally into particle concentrations that resulted in full coverage. To demonstrate that varying the concentration ratio of SiO_2 NPs *versus* PSL NPs results in incomplete coverage of the PSL NPs, the concentration of SiO_2 NPs was reduced with the results shown in Fig. 4, and Fig. S6, ESI.†

The formation of supraparticles by using colloidally stable nanoparticles can be initiated by balancing the repulsive and attractive forces.[63–68] Decoration of (large) nanoparticles with (small) nanoparticles continues as long as attractive interactions between the nanoparticles are stronger than their repulsive counterparts.[65] As an example, this phenomenon is illustrated in Fig. 4 where a series of cryoTEM images shows the gradual increase of surface coverage of PSL NPs with increasing SiO_2 NP concentration. Varying concentrations of 30 nm SiO_2 NPs were utilized to form the partially covered AB supraparticles seen in Fig. 4, more specifically, number ratios of SiO_2 NPs and PSL NPs adjusted to 2 (7 μl SiO_2 NPs/10 μl PSL NPs), 10 (33 μl SiO_2 NPs/10 μl PSL NPs), and 20 (65 μl SiO_2 NPs/10 μl PSL NPs), respectively. While at low concentration only three SiO_2 NPs were attached to the surface of one PSL NP, the surface coverage increases with increasing concentration. To that end, it is crucial to realize that if the attractive interactions are too strong in the system, aggregates will be formed that eventually result in the precipitation of macroscopic agglomerates (Fig. S6, ESI†).[66,67]

The self-assembly of small nanoparticles on the surface of the large nanoparticles terminates upon reaching equilibrium between attractive and repulsive interactions.[65] The electrostatic interaction between nanoparticles can be used as a tool to regulate their self-assembly[69–75] as these interactions are very sensitive to the ionic strength and pH of the solution, providing

possibilities to tailor their magnitude and control the formation process. While a balance between attractive and repulsive interactions for individual nanoparticles is a key issue, several other important parameters, such as the concentration of the particles in the mixture, also play a crucial role to obtain the desired supraparticles. It is clear from Fig. 4 and Fig. S6 (ESI†) that the formation of supraparticles has stopped due to the lack of sufficient SiO_2 NPs being present in the mixture. Here the time granted for the formation of fully covered supraparticles was 1 week, while the attractive interaction between the SiO_2 NPs and PSL NPs was optimal as pH 2 is the optimum condition for the formation of fully covered supraparticles, as shown in Fig. 1 and 2. In fact, as long as the pH of the system is kept at 2, the supraparticles remain stable in the solution without forming excessive agglomerates. This, in principle, allows the organic and inorganic nanoparticles to form supraparticles and eventually reach the equilibrium.

As mentioned before, after landing on the surface of PSL NPs, we assumed that a specific SiO_2 NP is immobile, thereby occupying a random but fixed position on the surface. Assuming mobility, one would expect a coverage of the SiO_2 NPs over the PSL NP with the average nearest-neighbor distance of SiO_2 NPs maximized at any degree of coverage. Examining several partially covered supraparticles, it became clear that the nearest-neighbor distances of SiO_2 NPs vary considerably. For non-movable particles, the bonding energy should be several times kT, where kT represents the thermal energy. For lateral mobility on the PSL surface, on the other hand, the bonding energy should be sufficient to keep the particles attached but small enough allowing thermally induced motion over the surface. In essence, a too strong attachment prevents lateral mobility. We conclude therefore from the observed irregular coverage that, once a SiO_2 NP has landed under suitable solution conditions, the SiO_2 NPs are immobile. This inherent feature of SiO_2 NPs is exploited to our advantage to create supraparticles with two different types of small NPs, a type of supraparticle which we termed ABC supraparticles.

In the light of the information that we gained for the formation of AB supraparticles and stable partially covered AB supraparticles, we decided to create more complex ternary ABC supraparticles by employing iron oxide nanoparticles in addition to silica nanoparticles. Different types of small nanoparticles decorating the surface of a large nanoparticle can pave the way for new materials with physico-chemical and morphological properties that are tailored for specific applications. Such an example can be found in the literature where it has been shown that two metallic nanoparticles can coexist on the surface of a larger inorganic nanoparticle,[20] however, the lack of size control of the metallic nanoparticles due to the *ex situ* approach used for their formation hampers, as indicated in the introduction, the possibilities of having a well-controlled coverage. Additionally, as supraparticles are normally considered to be uniform in terms of type and size of the small nanoparticles covering the large nanoparticle, surface heterogeneities in terms of the size of the small nanoparticles can play a detrimental role in reaching super hydrophobicity.[76]
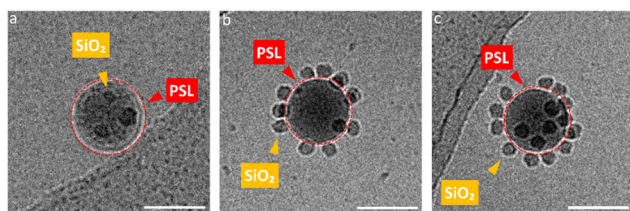

Fig. 4 CryoTEM analysis of stepwise coverage of a single 100 nm PSL NP with SiO_2 NPs with a diameter of 24 nm with increasing concentrations at pH 2. Scale bars are 100 nm.

Here, by benefiting from controllable adsorption, partially covered stable supraparticles are used to create a supraparticle system where either two different sizes or two different types of small nanoparticles coexist on the surface of large PSL NPs. To achieve our goals, we initially employed five different inorganic nanoparticle systems: 10 nm SiO_2, 30 nm SiO_2, 30 nm TiO_2, 10 nm Fe_3O_4, and 30 nm Fe_3O_4. After some preliminary experiments, the 30 nm TiO_2 and 10 nm Fe_3O_4 NPs appeared to be unsuitable for the formation of ABC supraparticles (see Fig. S7 and S8, ESI†). We omit further discussion of these efforts and focus on the 10 nm SiO_2, 30 nm SiO_2 and 30 nm Fe_3O_4 NPs.

One of the crucial parameters governing the self-assembly of small nanoparticles on the surface of large particles is the total surface charge of the building blocks that are utilized and depending on the number of SiO_2 NPs in the system, the total surface charge of stable partially covered supraparticles can be adjusted. In order to create the partially covered supraparticles with the most effective interaction range together with the most suitable free interstitial positions on the surface, two different partially covered supraparticles were formed and further characterized via cryoTEM and DLS to determine their structural and intrinsic properties (Fig. S9, ESI†). Considering that the zeta potential of PSL NPs, SiO_2 NPs, and fully covered supraparticles are −45 mV, +27 mV, and +23 mV, respectively, the zeta potential of partially covered supraparticles was adjusted by controlling the concentration of silica nanoparticles to have a negative value as they were intended to be used as templates for further experiments. Moreover, a delicate balance in terms of surface potential, as reflected in the zeta potential, and the number of small nanoparticles on the surface of partially covered supraparticles needs to be arranged so that, while partially covered supraparticles are negatively charged, they should, to regulate the self-assembly of newly added NPs, still provide sufficient electrostatic interactions and offer sufficient interstitial empty spaces. Here, it is important to mention that, while both partially covered supraparticles with zeta potentials of −36 mV and −13 mV provide sufficient empty space for the third building block (C), having finally an about equal coverage of B and C particles, partially covered supraparticles with a zeta potential of −13 mV are required. Nevertheless, two partially covered supraparticle systems with zeta potentials of −36 mV and −13 mV were prepared by altering the number of SiO_2 NPs on the surface of PSL NPs (Fig. S9, ESI†), but the one having −13 mV was chosen for further experiments for the above-mentioned reason.

Similar characterization steps were applied to the 10 nm SiO_2 and 30 nm Fe_3O_4 NPs in order to determine the size and zeta potential of these building blocks. CryoTEM and conventional dry TEM results (Fig. S4, ESI†) demonstrated that the size distribution of 10 nm SiO_2 and 30 nm Fe_3O_4 are suitable to utilize them as building blocks for the formation of ABC supraparticles. We initially formed partially covered supraparticles by utilizing PSL NPs (A) as core particles and by using either 30 nm Fe_3O_4 (B) or 30 nm SiO_2 NPs (B) as the first inorganic building block. Thereafter, by taking advantage of the remaining electrostatic attraction for newly added inorganic

building blocks (C), 10 nm SiO_2 NPs were introduced to the system.[25,55]

Besides the electrostatic interactions, also the mixing ratio of the newly added nanoparticles must be considered. The number of newly added NPs needed to ensure dense coverage on a core particle is estimated by calculating how many newly added nanoparticles can be fitted into the interstitial empty space of already partially covered supraparticles. Interestingly, we observed a dependence on the order of addition of the 10 nm SiO_2 and 30 nm SiO_2 NPs. The partially covered AB supraparticles made by using 10 nm SiO_2 NPs do not allow newly added 30 nm SiO_2 NPs to attach to the surface of partially covered supraparticles (Fig. S10 and S11, ESI†). Fig. S10 (ESI†) shows that newly added 30 nm SiO_2 NPs remained free in the solution and could not attach to the surface of supraparticles are marked with red circles, while newly added 30 nm SiO_2 NPs of which very few attached to the surface of supraparticles are marked with yellow circles. Hence, we used a different approach to create ABC supraparticles with 10 nm and 30 nm SiO_2 NPs. Instead of forming partially covered supraparticles with 10 nm SiO_2 NPs, we employed 30 nm SiO_2 NPs to form partially covered stable supraparticles and then added 10 nm SiO_2 NPs. CryoTEM results indicate that, while full surface coverage was not achieved, a considerable amount of both size of SiO_2 NPs coexisted on the core particle surface was successfully obtained (Fig. 5, SM4–7).

Moreover, to demonstrate the versatility of our approach to create ABC supraparticles with controlled surface topography, we made stable partially covered supraparticles by using 30 nm Fe_3O_4 NPs instead of using SiO_2 NPs and thereafter initiate the formation of dual coverage supraparticles by adding 10 nm SiO_2 NPs. CryoTEM results demonstrate that partially covered supraparticles with 30 nm Fe_3O_4 NPs are formed successfully (Fig. S12, ESI†). Similarly, CryoTEM indicates that by thereafter adjusting the number of 10 nm SiO_2 NPs added to the system, ABC supraparticles were formed (Fig. 6, SM8–11).

Interestingly, while 10 nm SiO_2 NPs kicked out the already attached 30 nm SiO_2 NPs upon landing on the surface of PSL
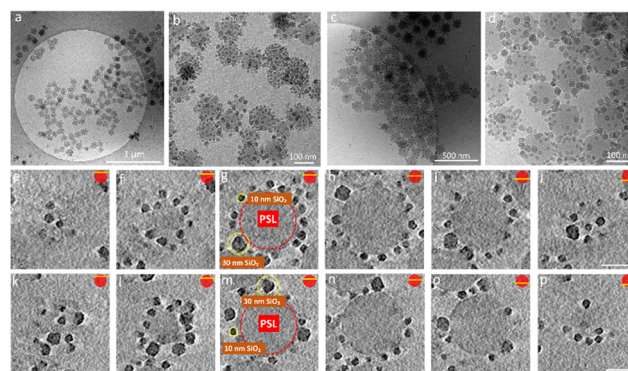

Fig. 5 CryoTEM images of ABC supraparticles created by employing 10 nm and 30 nm SiO_2 NPs (a–d). Cross-sections at different heights in two representative ABC supraparticles as obtained from cryoET reconstructions (e–p) demonstrate that the PSL nanoparticle is covered with different sizes of SiO_2 NPs. Scale bars = 100 nm.
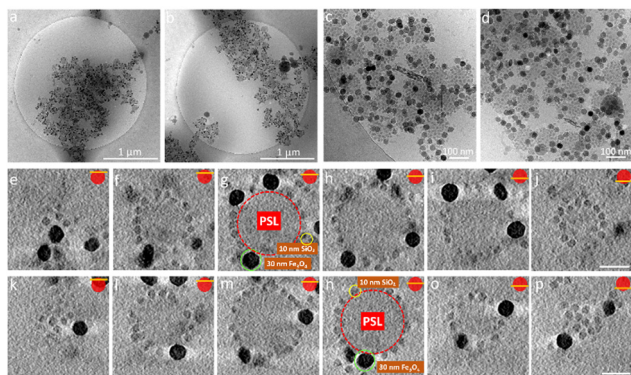
Fig. 6 CryoTEM images of ABC supraparticles created by employing 10 nm SiO_2 and 30 nm Fe_3O_4 NPs (a–d). Cross-sections at different heights in two representative ABC supraparticles as obtained from cryoET reconstructions (e–p) demonstrate that the PSL nanoparticle is covered with different sizes and types of inorganic nanoparticles. Scale bars = 100 nm.

NPs, making it impossible to fully cover the surface, the same 10 nm SiO_2 NPs did not trigger such an effect upon landing on the surface of partially covered PSL NPs which are created by using 30 nm Fe_3O_4 NPs.

At this point it is important to indicate that both enthalpic and entropic contributions play a crucial role in reaching equilibrium structures, in our case the supraparticles. We consider that, regardless of their size, either 10 nm or 30 nm SiO_2 NPs, these NPs have a similar surface charge values, as reflected by their zeta potential, due to the same surface modification method that was used to functionalize them. Therefore, entropy rather than enthalpy plays the dominant role in the formation of dual coverage supraparticles upon mixing 10 and 30 nm SiO_2 NPs. To estimate the change of entropy upon self-assembly, Flory–Huggins solution theory was employed which yields for the entropy of mixing

$$\Delta_{mix}S = -nR(\varphi_1 \ln \varphi_1 + \varphi_2 \ln \varphi_2) \qquad (1)$$

with n being the total number of the species in the system, R the ideal gas constant and φ the volume fraction of the species. Combining entropic estimates using the Flory–Huggins expression with enthalpic estimates in which the bonding energy for supraparticles is calculated using DLVO theory, can explain this behavior. Such an estimate indicates that the bonding energy of the Fe_3O_4 NPs is sufficiently large to balance the entropy change due to SiO_2 NP adsorption. For a detailed calculation, see ESI.†

Several aspects of supraparticles described in this work were investigated previously[25,55] and it is important to state that all the experiments including cryoTEM, cryoET, size, and zeta potential measurement were conducted anew for the current study (for further representative cryoET results, see SM12–16). As overlapping experiments showed very similar results, this demonstrates the highly reproducible nature of these supraparticles. While, as described, well-controlled supraparticles can be realized, from a mass production point of view, our system clearly needs further optimization to produce larger quantities.

Conclusions

In this paper, we discussed the formation of binary AB and ternary ABC supraparticles by employing a wide range of organic and inorganic nanoparticles in terms of diameters and types. CryoTEM investigations show that AB supraparticles can be realized with core PSL NPs with a diameter between 80 nm and 450 nm with a layer of SiO_2 NPs using a range of 1/2 to 1/15 to PSL NPs diameter. Comparing the coverage with theoretical estimates, we conclude that for all systems maximum coverage was obtained. For low size ratio, the coordination number of the SiO_2 NPs on the PSL NP varies between 3 and 7, while for larger ratio mainly 5, 6 and 7-fold coordination occurs with an increasing fraction of 6-fold coordination. The balance between attraction and repulsion determines the structural stability of a supraparticle: the attraction should be strong enough to secure stability of the shell particles on the core, while the repulsion co-determines the spacing of the shell particles on the core. However, in the case of attachment to a surface, the question is also whether the particles attached are still mobile (but having sufficient attraction to keep a particle stable) or not (having such a strong attraction so that mobility is absent). We have provided arguments that the particles are not mobile and if this "localization" is strong enough, other interactions are consequently of lesser importance. In this case a regular spacing of the shell particles over the core is not expected. Moreover, we demonstrate that coverage of the PSL NPs can be controlled by adjusting the concentration of SiO_2 NPs which allows us to create partially covered stable supraparticles. Thereafter, these partially covered stable AB supraparticles are used to form a next level ABC supraparticles comprising a core (A) particle covered with a shell of different (B and C) particles. We conclude that electrostatically driven adsorption of different inorganic nanoparticles onto partially covered supraparticles is a robust strategy to create ternary ABC supraparticles. This extended toolbox for supraparticle assembly, that can be customized for the design of a wide range of different building blocks, can be employed to advantage to create next generation materials.

Author contributions

E. D. E. and G. d. W. conceived the project; E. D. E., M. A. M., M. M. J. v. R., and B. M. O. conducted the experiments and data analysis, and discussed with H. F. and GdW. All authors contributed to review and editing of the manuscript.

Conflicts of interest

There are no conflicts to declare.

Acknowledgements

References

1 L. M. Liz-Marzán, C. J. Murphy and J. Wang, *Chem. Soc. Rev.*, 2014, **43**, 3820–3822.

2 P. K. Jain, X. Huang, I. H. El-Sayed and M. A. El-Sayed, *Plasmonics*, 2007, **2**, 107–118.

3 R. Schlögl and S. B. Abd Hamid, *Angew. Chem., Int. Ed.*, 2004, **43**, 1628–1637.

4 P. C. Chen, G. Liu, Y. Zhou, K. A. Brown, N. Chernyak, J. L. Hedrick, S. He, Z. Xie, Q. Y. Lin, V. P. Dravid, S. A. O'Neill-Slawecki and C. A. Mirkin, *J. Am. Chem. Soc.*, 2015, **137**, 9167–9173.

5 Z. Tang and N. A. Kotov, *Adv. Mater.*, 2005, **17**, 951–962.

6 K. McNamara and S. A. M. Tofail, *Adv. Phys.: X*, 2017, **2**, 54–88.

7 A. H. Lu, E. L. Salabas and F. Schüth, *Angew. Chem., Int. Ed.*, 2007, **46**, 1222–1244.

8 M. Haase and H. Schäfer, *Angew. Chem., Int. Ed.*, 2011, **50**, 5808–5829.

9 Y. Shirasaki, G. J. Supran, M. G. Bawendi and V. Bulović, *Nat. Photonics*, 2013, **7**, 13–23.

10 M. Nguyen, N. Felidj and C. Mangeney, *Chem. Mater.*, 2016, **28**, 3564–3577.

11 A. Le Beulze, S. Gomez-Graña, H. Gehan, S. Mornet, S. Ravaine, M. Correa-Duarte, L. Guerrini, R. A. Alvarez-Puebla, E. Duguet, E. Pertreux, A. Crut, P. Maioli, F. Vallée, N. Del Fatti, O. Ersen and M. Treguer-Delapierre, *Nanoscale*, 2017, **9**, 5725–5736.

12 W. Ming, D. Wu, R. van Benthem and G. de With, *Nano Lett.*, 2005, **5**, 2298–2301.

13 Z. Qian, S. P. Hastings, C. Li, B. Edward, C. K. Mcginn, N. Engheta, Z. Fakhraai and S. Park, *ACS Nano*, 2015, 1263–1270.

14 S. C. Glotzer and M. J. Solomon, *Nat. Mater.*, 2007, **6**, 557–562.

15 F. Li, D. P. Josephson and A. Stein, *Angew. Chem., Int. Ed.*, 2011, **50**, 360–388.

16 P. F. Damasceno, M. Engel and S. C. Glotzer, *Science*, 2012, **337**, 453–457.

17 V. N. Manoharan, *Science*, 2015, **349**, 1253751.

18 A. B. Pawar and I. Kretzschmar, *Macromol. Rapid Commun.*, 2010, **31**, 150–168.

19 M. A. Boles, M. Engel and D. V. Talapin, *Chem. Rev.*, 2016, **116**, 11220–11289.

20 T. Shirman, J. Lattimer, M. Luneau, E. Shirman, C. Reece, M. Aizenberg, R. J. Madix, J. Aizenberg and C. M. Friend, *Chem. – Eur. J.*, 2018, **24**, 1833–1837.

21 M. P. Kim, D. J. Kang, D. W. Jung, A. G. Kannan, K. H. Kim, K. H. Ku, S. G. Jang, W. S. Chae, G. R. Yi and B. J. Kim, *ACS Nano*, 2012, **6**, 2750–2757.

22 F. Meder, S. S. Thomas, T. Bollhorst and K. A. Dawson, *Nano Lett.*, 2018, **18**, 2511–2518.

23 C. S. Wagner, S. Shehata, K. Henzler, J. Yuan and A. Wittemann, *J. Colloid Interface Sci.*, 2011, **355**, 115–123.

24 S. Saxena and L. Andrew Lyon, *J. Colloid Interface Sci.*, 2015, **455**, 93–100.

25 E. D. Eren, M. A. Moradi, H. Friedrich and G. de With, *Nano Lett.*, 2021, **21**, 2232–2239.

26 S. Harley, D. W. Thompson and B. Vincent, *Colloids Surf.*, 1992, **62**, 163–176.

27 F. Luckham, *J. Chem. Soc., Faraday Trans. 1*, 1980, **76**, 674–682.

28 A. Dokoutchaev, J. Thomas James, S. C. Koene, S. Pathak, G. K. Surya Prakash and M. E. Thompson, *Chem. Mater.*, 1999, **11**, 2389–2399.

29 M. Kanahara, M. Shimomura and H. Yabu, *Soft Matter*, 2014, **10**, 275–280.

30 M. Oćwieja, D. Lupa and Z. Adamczyk, *Langmuir*, 2018, **34**, 8489–8498.

31 X. Li and J. He, *ACS Appl. Mater. Interfaces*, 2012, **4**, 2204–2211.

32 B. G. P. van Ravensteijn and W. K. Kegel, *Langmuir*, 2014, **30**, 10590–10599.

33 M. Sadowska, Z. Adamczyk and M. Nattich-Rak, *J. Colloid Interface Sci.*, 2017, **505**, 509–518.

34 M. Sadowska, Z. Adamczyk, M. Oćwieja and M. Nattich-Rak, *Colloids Surf., A*, 2016, **499**, 1–9.

35 M. Zanini, C. P. Hsu, T. Magrini, E. Marini and L. Isa, *Colloids Surf., A*, 2017, **532**, 116–124.

36 M. Zanini, C. Marschelke, S. E. Anachkov, E. Marini, A. Synytska and L. Isa, *Nat. Commun.*, 2017, **8**, 1–9.

37 M. J. Bowick and L. Giomi, *Adv. Phys.*, 2009, **58**, 449–563.

38 P. Lipowsky, M. J. Bowick, J. H. Meinke, D. R. Nelson and A. R. Bausch, *Nat. Mater.*, 2005, **4**, 407–411.

39 A. R. Bausch, *Science*, 2003, **299**, 1716–1718.

40 R. F. Curl and R. E. Smalley, *Science*, 1985, **242**, 1017–1022.

41 Y. Quo, N. Karasawa and W. A. Goddard, *Nature*, 1991, **351**, 464–467.

42 H. W. Kroto, J. R. Heath, S. C. O'Brien and R. E. Smalley, *Nature*, 1985, **318**, 162–163.

43 M. F. Jarrold, *Nature*, 2000, **407**, 26–27.

44 J. P. Patterson, Y. Xu, M. A. Moradi, N. A. J. M. Sommerdijk and H. Friedrich, *Acc. Chem. Res.*, 2017, **50**, 1495–1501.

45 G. Mirabello, A. Keizer, P. H. H. Bomans, A. Kovács, R. E. Dunin-Borkowski, N. A. J. M. Sommerdijk and H. Friedrich, *Chem. Mater.*, 2019, **31**, 7320–7328.

46 G. Mirabello, A. Ianiro, P. H. H. Bomans, T. Yoda, A. Arakaki, H. Friedrich, G. de With and N. A. J. M. Sommerdijk, *Nat. Mater.*, 2020, **19**, 391–396.

47 C. C. M. C. Carcouët, M. W. P. van de Put, B. Mezari, P. C. M. M. Magusin, J. Laven, P. H. H. Bomans, H. Friedrich, A. C. C. Esteves, N. A. J. M. Sommerdijk, R. A. T. M. van Benthem and G. de With, *Nano Lett.*, 2014, **14**, 1433–1438.

48 B. M. Oosterlaken, M. M. J. van Rij, R. R. M. Joosten, P. H. H. Bomans, H. Friedrich and G. de With, *ACS Biomater. Sci. Eng.*, 2021, **7**, 3123–3131.

49 J. L. S. Milne, M. J. Borgnia, A. Bartesaghi, E. E. H. Tran, L. A. Earl, D. M. Schauder, J. Lengyel, J. Pierson, A. Patwardhan and S. Subramaniam, *FEBS J.*, 2013, **280**, 28–45.

50 N. D. Burrows and R. L. Penn, *Microsc. Microanal.*, 2013, **19**, 1542–1553.

51 J. Kuntsche, J. C. Horst and H. Bunjes, *Int. J. Pharm.*, 2011, **417**, 120–137.

52 G. Yu, R. Yan, C. Zhang, C. Mao and W. Jiang, *Small*, 2015, **11**, 5157–5163.

53 M. Turk and W. Baumeister, *FEBS Lett.*, 2020, **594**, 3243–3261.

54 P. L. Stewart, *Wiley Interdiscip. Rev.: Nanomed. Nanobiotechnol.*, 2017, **9**, e1417.

55 M. Moradi, E. D. Eren, M. Chiappini, S. Rzadkiewicz, M. Goudzwaard, M. M. J. van Rijt, A. D. A. Keizer, A. F. Routh, M. Dijkstra, G. de With, N. Sommerdijk, H. Friedrich and J. P. Patterson, *Nat. Mater.*, 2021, **20**, 541–547.

56 T. Yokoi, Y. Sakamoto, O. Terasaki, Y. Kubota, T. Okubo and T. Tatsumi, *J. Am. Chem. Soc.*, 2006, **128**, 13664–13665.

57 K. N. Pham, D. Fullston and K. Sagoe-Crentsil, *Aust. J. Chem.*, 2007, **60**, 662–666.

58 H. S. Jung, D. S. Moon and J. K. Lee, *J. Nanomater.*, 2012, **2012**, 1–8.

59 R. S. Shreedhara Murthy and D. E. Leyden, *Anal. Chem.*, 1986, **58**, 1228–1233.

60 R. G. Acres, A. V. Ellis, J. Alvino, C. E. Lenahan, D. A. Khodakov, G. F. Metha and G. G. Andersson, *J. Phys. Chem. C*, 2012, **116**, 6289–6297.

61 M. L. Mansfield, L. Rakesh and D. A. Tomalia, *J. Chem. Phys.*, 1996, **105**, 3245–3249.

62 M. J. Bowick, D. R. Nelson and A. Travesset, *Phys. Rev. B: Condens. Matter Mater. Phys.*, 2000, **62**, 8738–8751.

63 Y. Xia and Z. Tang, *Chem. Commun.*, 2012, **48**, 6320–6336.

64 M. Maas, C. C. Silvério, J. Laube and K. Rezwan, *J. Colloid Interface Sci.*, 2017, **501**, 256–266.

65 E. Piccinini, D. Pallarola, F. Battaglini and O. Azzaroni, *Mol. Syst. Des. Eng.*, 2016, **1**, 155–162.

66 N. A. Kotov, *J. Mater. Chem.*, 2011, **21**, 16673–16674.

67 A. M. Islam, B. Z. Chowdhry and M. J. Snowden, *Adv. Colloid Interface Sci.*, 1995, **62**, 109–136.

68 T. Wang, D. La Montagne, J. Lynch, J. Zhuang and Y. C. Cao, *Chem. Soc. Rev.*, 2013, **42**, 2804–2823.

69 C. S. Wagner, S. Shehata, K. Henzler, J. Yuan and A. Wittemann, *J. Colloid Interface Sci.*, 2011, **355**, 115–123.

70 S. L. Westcott, S. J. Oldenburg, T. R. Lee and N. J. Halas, *Langmuir*, 1998, **14**, 5396–5401.

71 M. A. Kostiainen, P. Hiekkataipale, A. Laiho, V. Lemieux, J. Seitsonen, J. Ruokolainen and P. Ceci, *Nat. Nanotechnol.*, 2013, **8**, 52–56.

72 A. F. Demirörs, J. C. P. Stiefelhagen, T. Vissers, F. Smallenburg, M. Dijkstra, A. Imhof and A. van Blaaderen, *Phys. Rev. X*, 2015, **5**, 1–12.

73 S. Zhang, Y. Shao, G. Yin and Y. Lin, *Angew. Chem., Int. Ed.*, 2010, **49**, 2211–2214.

74 P. Dušak, A. Mertelj, S. Kralj and D. Makovec, *J. Colloid Interface Sci.*, 2014, **438**, 235–243.

75 A. M. Kalsin, M. Fialkowski, M. Paszewski, S. K. Smoukov, K. J. M. Bishop and B. A. Grzybowski, *Science*, 2006, **312**, 420–424.

76 C. C. M. C. Carcouët, A. C. C. Esteves, M. M. R. M. Hendrix, R. A. T. M. van Benthem and G. de With, *Adv. Funct. Mater.*, 2014, **24**, 5745–5752.